December 2015

Label Free Analysis of Native Planktonic P. aeruginosa cells and Growth Media by Near Infrared (NIR) Binary Spectronephelometry (BSN)

Steven Ortiz
Syracuse University

Abstract

Current noninvasive methods are unable to continuously and simultaneously monitor the concentration of cells and chemical components that define the state of native bacterial cultures because of the changing turbidity. We seek to solve this problem without subjecting the growing culture to the risk of contamination afforded by physical sampling. The Binary Spectronephelometry (BSN) algorithm uses laser induced emission to probe mildly turbid media. A training set spanning the linear range of elastic emission (EE) i.e. physical scattering and inelastic emission (IE) i.e. fluorescence and Raman emission was produced with varying concentrations of bacteria and standard media using a modified commercial Raman spectrometer. The training set results confirmed the linear dependence of the EE and IE signals on the concentration of bacteria cells as determined by the known dilutions and the optical density at 600nm (OD_{600}) thus confirming the basic assumptions of the algorithm and simultaneously calibrating the algorithm. *Pseudomonas aeruginosa* (*PA*) is a bacterium capable of forming biofilms that allow survival in various conditions and transmittance from surfaces to person causing infection. *PA* cultures were monitored for several hours producing quantitative growth/decay curves for the bacteria concentration and the medium concentration. This was considered a challenging application of the algorithm because of the increase in viscosity and schlieren effects characteristic of *PA* with increasing culture time. Simultaneously obtained Raman spectra quantitatively demonstrate the conversion of feedstock i.e. glucose into product i.e. biomass in the form of bacterial membrane phospholipids, information concerning the chemical state of the medium and the organisms. We discuss these results in the context of various applications and future research and development.

Label Free Analysis of Native Planktonic *P. aeruginosa* cells and Growth Media by Near Infrared (NIR) Binary Spectronephelometry (BSN)

by

Steven Ortiz

B.S., Rhode Island College, 2012

Thesis

Submitted in partial fulfillment of the requirements for the degree of

Master of Science in *Chemistry*.

Syracuse University

December 2015

Acknowledgements

The assistance from Hewen Zheng of the Luk Group and Professor Luk, Professor Goodisman, Richard McDonough and Paul Dent was invaluable and appreciated. The funding provided by LighTouch, Inc. and instrumental support from Lambda Solutions Inc. for this and other research studies is also very much appreciated.

Table of Contents

List of Illustrative Material

Introduction

Binary Spectronephelometry

The usual *in situ* method employed by biochemists for determining the concentration of bacteria in media solution is the attenuation of light passing through a sample at 600nm also known as the optical density or OD_{600}. However this method gives users limited information, only the concentration of cells in solution and no chemical information such as media composition or how it might be changing. It is also susceptible to unwanted artifacts due to absorption or scattering losses not related to the bacteria concentration. Near Infrared (NIR) Binary Spectronephelometry (BSN) was developed to determine bacteria concentration simultaneously with analyzing the media chemically e.g. glucose or other feedstock concentration. Using a modified Raman spectrometer, one incident laser produces an emission spectrum containing two types of light scattering and fluorescence. The first is the Elastic Emission (EE) that is displayed in the Rayleigh line region of the spectrum. As the light from the laser passes through the sample some of the photons experience physical i.e. Rayleigh or Mie scattering producing no shift in wavelength and appearing in the spectrum as a narrow peak. The second type of signal is Inelastic Emission (IE) and arises from inelastic interactions between the photon and molecules. The molecules absorb the energy from the laser photons and fluoresce or change their vibrational mode, in either case causing light to scatter with a shift in wavelength. This can be seen in the Raman and fluorescence region of the spectrum as shown below in Figure 1 and the apparatus is depicted schematically in Figure2.

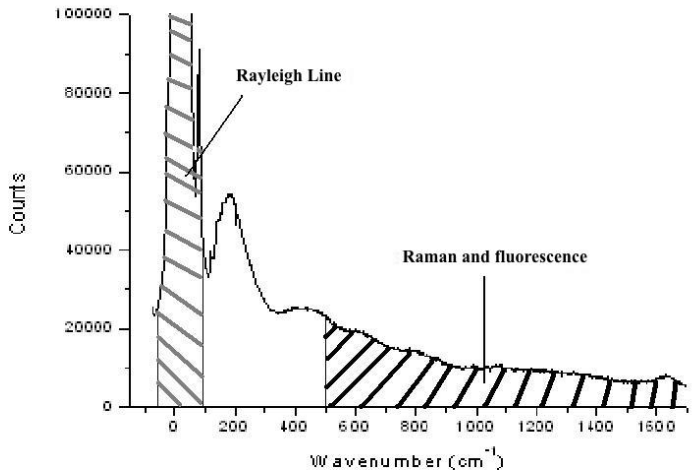

Fig. 1: Spectrum showing the wavenumber vs. photon count, the Rayleigh line (EE) and the Raman and fluorescence (IE) regions.

In order to obtain the information we want from the EE and IE an algorithm was developed by Chaiken and Goodisman.[1] The algorithm relates the number of photons scattered elastically and inelastically to both the volume fraction of bacteria (ϕ_{bac}) and the volume fraction of media (ϕ_{med}). It was necessary to develop the algorithm because the bacteria cells not only contribute to the EE scattering but since the cells themselves are composed of molecules such as lipids, saccharides and DNA, they affect the IE signal as well. The liquid medium phase also contributes both EE and IE and we explore the effect of these multiple sources on the efficacy of the algorithm.

The sum of the volume fractions of the bacteria, media and the scattered light caused by the bottom of the cuvette accounts for the entire volume of the solution and is set to equal one. Furthermore, as we show below, typical medium and growing conditions produce elastic scattering from debris in the medium.

$$1 = \phi_{bac} + \phi_{med} + \phi_{cuv} \quad [1]$$

And the sum of the changes of these volume fractions will be zero since the total volume is constant.

$$0 = d\phi_{bac} + d\phi_{med} + d\phi_{cuv} \quad [2]$$

From radiation transfer theory,[2] in principle it is always possible to find a linear range for propagation losses in turbid solutions between zero and some higher concentration of physical scatterer i.e. bacteria concentration. Once experimental data has confirmed that the relationship between the volume fractions and the scattered light is linear for a specific range of concentrations, then equations 3 and 4 apply giving the relationship between the EE and IE signals to each of the volume fractions.

$$EE = \vartheta_1 + \vartheta_2\phi_{bac} + \vartheta_3\phi_{med} \quad [3]$$

$$IE = \vartheta_4 + \vartheta_5\phi_{bac} + \vartheta_6\phi_{med} \quad [4]$$

As stated before the bacteria cells contribute to both the EE and IE and the media could potentially do the same so both independent variables are needed in calculating both the EE and IE. As long as the causes of EE and IE are physically independent processes, Equations 3 and 4 are linearly independent. Hence they can be algebraically inverted so that the measured

quantities (EE and IE) are the independent variables and the volume fractions of bacteria and media can be determined as shown in equations 5 and 6.

$$\phi_{bac} = a + b(EE) + c(IE) \qquad [5]$$

$$\phi_{med} = d + e(EE) + f(IE) \qquad [6]$$

The coefficients $a$through f are found experimentally by measuring EE and IE on a training set of varying concentrations of bacteria and media, using e.g. phosphate buffered saline (PBS) to adjust volume and media fractions as needed. With actual measurements, geometric and other practical issues are incorporated empirically into the training set. A bi-linear regression of e.g. ϕ_{bac} on EE and IE produces parameters a-c etc.

The choice of reference solutions to calibrate the algorithm with can accentuate the ability to observe small changes in specific characteristics. For example, we may anticipate that a real culture may produce particulate debris that scatters differently from the bacteria themselves. By choosing to include or exclude such particulates e.g. by filtration from the media during calibration we could "build-in" the EE produced by the media particulates. We might minimize interference in measuring the number density of bacteria although that could be completely ameliorated if the bacteria and particulates each produced distinctive Raman features.

A further trade-off involves the choice of the linear range over which to calibrate the algorithm. The more narrow the range and the lower the average turbidity over the range the better the

linearity. But if utility requires a broader range, or that it extend to higher turbidity e.g. for bacteria concentration, some systematic error may be acceptable. For *in vivo* systems, maintaining homeostasis is a driving force and the ability to monitor a narrow range of parameter space surrounding the optimal homeostasis conditions may be the only requirement to be clinically useful.[1]

Pseudomonas aeruginosa

Pseudomonas aeruginosa or *P. aeruginosa* (*PA*) is a gram-negative bacterium capable of organizing individual cells into an aggregate that form a biofilm protecting the collective from harsh environmental conditions.[3] *PA* is also a pathogen capable of causing infections in patients with immune compromised respiratory diseases like cystic fibrosis (CF) and chronic obstructive pulmonary disease (COPD) as well as people with physical trauma such as burns and abrasions.[4] Among patients with immunosuppressed diseases the mortality rate from *PA* infections is 40% to 60%, including patients in the burn and palliative care units in hospitals.[5] In the United States over 200,000 cases per year of severe infections arising from hospital visits alone have been reported with *PA* being the leading causative agent.[6]

The method, in which *PA* infections occur, is by forming biofilms onto biological surfaces such as bronchial tissue. Biofilms are aggregates of bacterial cells encased in a substance consisting of polysaccharides, eDNA, proteins, fimbriae and flagella that are secreted by the cells.[7,8,9] Another characteristic of *PA* that is of concern to scientists is its capability to survive in pure water. Whereas most organisms will experience cell rupture from the change in osmotic pressure *PA* will survive by forming biofilms to protect the bulk of the population and allow it survive with

little nutrients.[10] It is this same protection from hostile environments that makes these types of bacterial infections impervious to most antibiotic drugs and difficult to treat. The outer matrix of the biofilm does not permit drug molecules to reach the population of bacterial cells below the matrix that would cause cell death and interrupt the biofilm functions.

While the biofilm is intact it has many dynamic characteristics and cells that occupy different regions of the biofilm execute different metabolic and theoretically pathogenic functions. This has caused some scientists to believe that there is a connection between single-cell bacteria and more complex multi-cellular organisms and studying such biofilms can reveal details about the evolution of intricate biological systems.[8] Determining the progression from planktonic cells (free-roaming) to sessile cells (surface-attached) for the origination of biofilm assembly can contribute to the discovery of treatments for biofilm related illnesses and provide evidence for evolutionary theories. Providing researchers with a more efficient tool for studying *PA* cells and their environment can reveal more information on their behavior as they transition from planktonic to sessile cells.

There have been studies that involve spectroscopic analyses of *PA*; some of these studies use Surface Enhanced Raman Scattering (SERS) or Raman microscopy that can be utilized to identify bacteria at the single cell level.[5] The current technique for determining the concentration of bacterial cells is by measuring OD_{600} but this method provides no information on the medium. Crystal violet (CV) dye assay is used to determine the thickness of biofilm formed by *PA*. The dye is diffused through the cell membranes, then washed with a saline solution to remove excess CV and analyzed through UV-Vis spectroscopy.[11] However this process is limited because the

diffusion of CV into the biofilm is random and the number of wash cycles varies from group to group, all of which can affect the data collected and make this process time consuming. The purpose of this research is to determine whether light scattering and the BSN algorithm can be used to monitor quantitatively the physical and chemical environment of viable bacterial cells in solution.

Experimental

Raman Spectrometer

All samples were analyzed using both a Perkin-Elmer 950 Lambda UV-Vis spectrometer to obtain OD_{600} and a custom-made 785nm excitation Raman spectrometer. Figure 2 schematically shows the setup of the Raman instrument, the incident light path passes through a clean-up filter and then a collimator lens. The light is then reflected downward by a 45° angled mirror through a 3 mm aperture drilled through a second downward facing 45° angled metal mirror and focused several millimeters below the surface of the sample solution. With non-turbid samples the laser light impinges on the bottom of the cuvette. Some penetrates both the front and back surfaces of the cuvette bottom and enters a Wood's Horn. The rest is reflected upwards. With no turbidity the laser spot is roughly 3 mm in diameter on the bottom of the cuvette but the base of the cuvette is tilted so that the majority of the specular reflection is spatially filtered out of the collection optics train. The back-scattered EE and IE light is reflected by the mirror, notch-filtered to remove residual incident laser light, and dispersed by a Kaiser® f~1.4 Holospec spectrograph onto an Andor® Charge-Coupled Device (CCD) camera that measures intensities versus the wavelength shift.

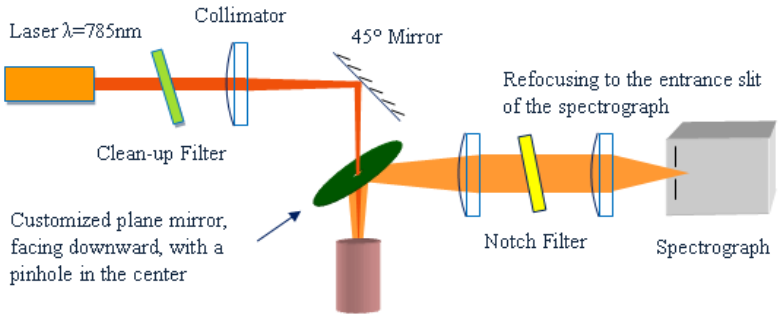

Fig. 2: The instrument setup for the custom made Raman spectrometer with an excitation wavelength of 785nm.

The CCD camera is thermoelectrically cooled to -55°C. The Andor® MCD operating system allows the user to select various scanning options such as mode, scan time, exposure time, etc. which controls the camera. For this research experiment two scanning modes were used during different phases, the first was 'Accumulation' mode that is a single scan for a set time (5 minutes) that produces one spectrum. And the second was 'Kinetic Series' mode, as the name suggests it produces a series of spectra each at a specific length of time (6 scans each for 5 minutes for a total scan time of 30 minutes). The dead time between scans is <1 second and between kinetic series is 15 minutes. For every experiment one or more 'Dark Current' spectra were recorded so that it could be subtracted from the sample spectra, this was done by completing an 'Accumulation' scan with the laser powered down. The UV-Vis spectrometer was used to measure the bacteria concentration for each sample at 600nm (OD_{600}) for comparison. For all scans performed using the Raman spectrometer the solvents (LB media and PBS) were filtered with Anatop® 0.2µm 25mm inorganic membrane filters into a clean beaker that is immediately covered with Parafilm®. This is done to ensure that the bacteria cells are the main objects in solution that contribute to the EE; the bacteria culture was not filtered. And all experiments were completed using a quartz cuvette (Amersil®101-QS; 1cm pathlength) with a low fluorescence background.

Calibration Curve and Training Set

Since the BSN algorithm is only rigorously valid across the linear propagation range, the first task was to find this range of concentrations for *PA* and LB media. The Luk research group, Department of Chemistry, Syracuse University, provided all *P. aeruginosa* cultures used in this research. The training set could be conveniently formed using serial half dilutions of a culture with Lysogeny Broth (LB) media and requiring a constant total volume of 3mL in the cuvette to produce a calibration curve. It is essential that each sample i.e. solution have the same volume since the reflection off the top of the solution produces a contribution to the collected EE. The notch filter was positioned in order to provide a numerical balance i.e. comparable signal to noise of EE and IE. This did not necessarily correspond to the optimal position of the filter to achieve the best Raman spectra but once calibrated, the system produces highly reproducible data. The system used for this pilot study is by no means optimized and a properly engineered system would possess much improved sensitivity, reproducibility and precision.

The OD_{600} of each of the diluted cultures were obtained, immediately followed by a Raman scan with the following settings. The scan was set to 'Accumulation' mode, the number of accumulations was 1500, exposure time was 0.2 seconds and the cycle time was 0.2 seconds, for a total scan time of five minutes. After subtracting the dark current, the sum of the signals from about $-7cm^{-1}$ to $50cm^{-1}$ was taken to calculate the signals contributed from the EE. The IE signals were calculated by summing up the signals from about $900cm^{-1}$ to the end of the spectrum i.e. about $1900cm^{-1}$, all calculations were performed using Microsoft Excel. The EE and IE signals

were then transferred to an OriginLabs Origin worksheet; this program was used to produce all graphs.

To obtain transient data as in Growth Curves the Raman spectrometer was setup with the following settings: Acquisition mode was Kinetic Series, Exposure Time was 0.2sec, Accumulate Cycle Time was 0.2sec, Number of Accumulations was 1500, Number in Kinetic Series was 6, the program should automatically set the Kinetic Cycle Time to 300sec. These settings will give a series of six scans each five minutes long for a total scan time of thirty minutes. A custom made cuvette holder was used, it was designed to allow heated water to circulate around the cuvette, a hot water thermostat was used to keep the solution at 37°C. At the side of the cuvette holder a modified magnetic stirrer was placed with the magnet nearly parallel with the closest vertical side of the cuvette.

To begin obtaining a growth curve, a culture of *PA* was diluted using LB media to an OD_{600} of about 0.02 to 0.03; 3.5mL of this diluted solution was placed into cuvette along with a tiny magnetic stir bar. Once the cuvette is placed into the cuvette holder the stirrer was powered on and the holder was raised to the highest position so that the light is focused consistently at the same position below the surface of the solution. After each 30-minute kinetic series 25µL of LB media was added to the cuvette to reduce the effect of evaporation of the solvent and after every two series or every hour the cuvette was removed and the OD_{600} taken. The data obtained from the growth curves were analyzed the same way as with the calibration curve, a dark current scan was taken before and after the experiment then the average of the two was subtracted from the spectra.

The volume fraction of bacteria is the volume that the bacteria cells occupy with respect to the volume of the entire solution. To calculate the volume fraction of bacteria an OD_{600} of 1 was set as 6.0×10^{8}cells/mL[12,13] and the average cell size was taken as $1.5\mu m$ in length (l) and $0.6\mu m$ wide (w).[14,15] Flow cytometry could also be used for calibration and we intend to explore that approach in future experiments. Using this information the average volume that the bacteria cells occupy was calculated using the equation below.

$$\phi_{bac} = \frac{Vol\ of\ Cells(mL)}{Vol\ of\ Solution(mL)} = \frac{(OD_{600})(6.0\times10^{-4})(2\pi w^{2}\times l)}{V_{sol}} \qquad [7]$$

Once the volume fraction of bacteria has been found for each solution in the calibration curve the Origin worksheet was used to create a graph of the EE and IE signals versus the volume fractions of the bacterial cultures. Figure 3 below shows the calibration curve that was used to determine the maximum bacterial concentration in the "linear" range i.e. Figure 4 which was found to correspond to an OD_{600} of about 0.4. Then a second calibration curve was produced with this maximum concentration to confirm that the range is in fact linear. We know that there will be some systemic error despite the high linear correlation but in appropriate cases it is a worthwhile trade off and can be ameliorated to some extent if a redundant signal is available e.g. Raman features that can be assigned to specific materials.

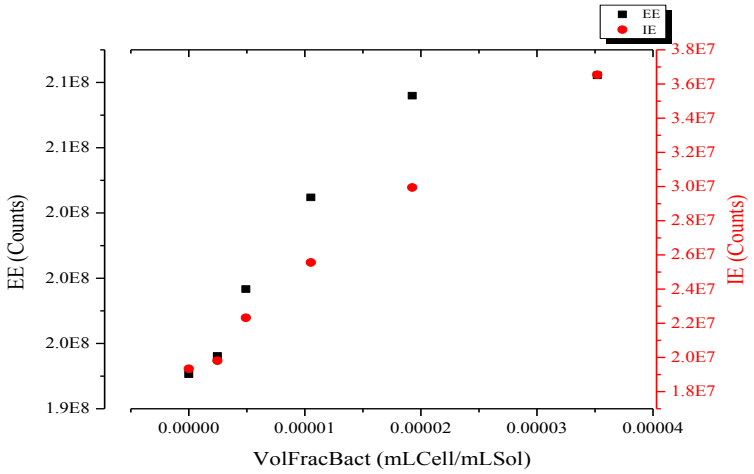

Fig. 3: Calibration Curve showing the EE and IE signals in photon counts versus the volume fraction of bacteria.

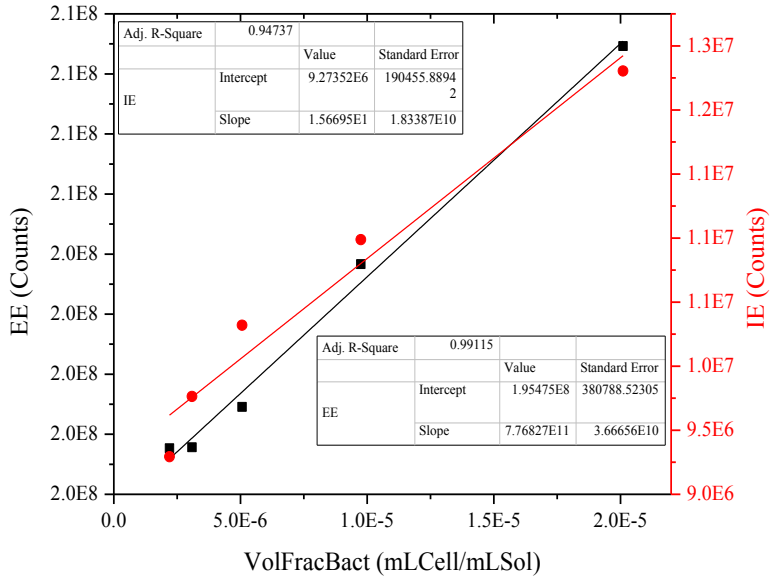

Fig. 4: The linear range of the calibration curve.

Next in the procedure was the development of a “training set” i.e. a series of solutions with systematically varying concentrations of bacteria culture, LB media and Phosphate Buffered

Saline (PBS) chosen to span the linear range. Starting with a recently grown bacteria culture we dilute it with LB media so that it has an OD_{600} of 0.4 or below. Then we prepare six solvents that will be used to dilute the culture in each series of the training set; the solvents are serial half dilutions of filtered LB media with PBS. Then each series involved half dilutions of the culture with the corresponding solvent to create a six by six training set, each with a total volume of 3mL. Each solution in the training set was analyzed by taking OD_{600} and BSN measurements i.e. EE and IE using the same settings as the calibration curve.

The training set data was collected, analyzed and graphed in the same manner as the calibration curve data, the following Figures 5-8 show the EE and IE signals as the concentration of both bacteria and LB media are independently changed. The training set is necessary so that the coefficients a through f in equations 5 and 6 i.e. the BSN algorithm can be determined using a bi-linear regression in the Origin program. Starting with the OD_{600} taken at the start of each series of the training set we calculated the concentration of each dilution. The solvent concentration was calculated by percent volume of half dilutions with PBS.

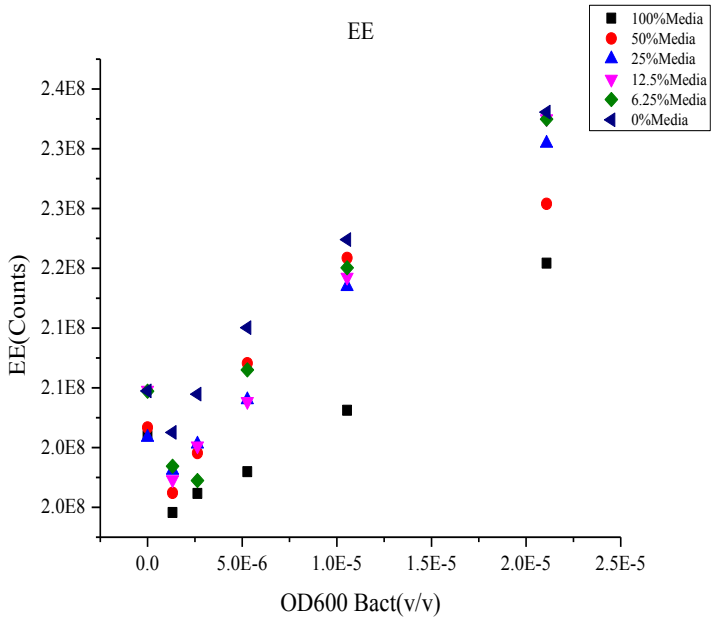

Fig. 5: A graph displaying the EE signal in photon counts versus the volume fraction of bacteria for each of the series in the training set.

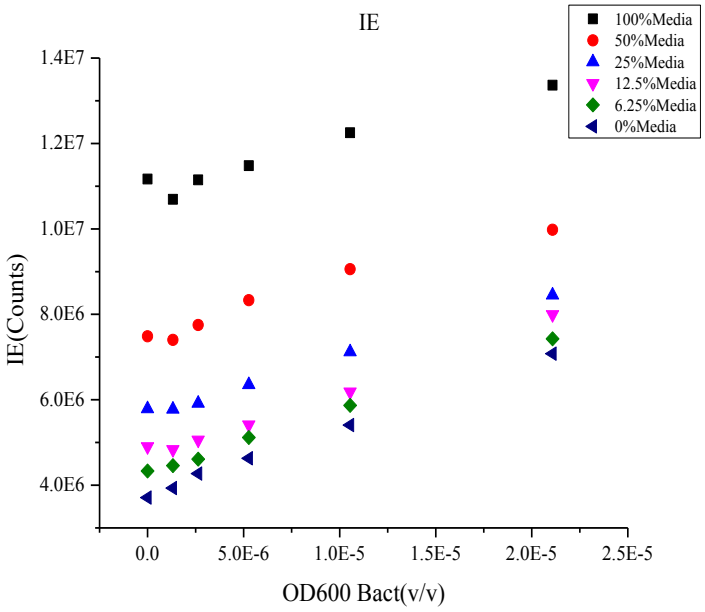

Fig. 6: A graph displaying the IE signal in photon counts versus the volume fraction of bacteria for each of the series in the training set.

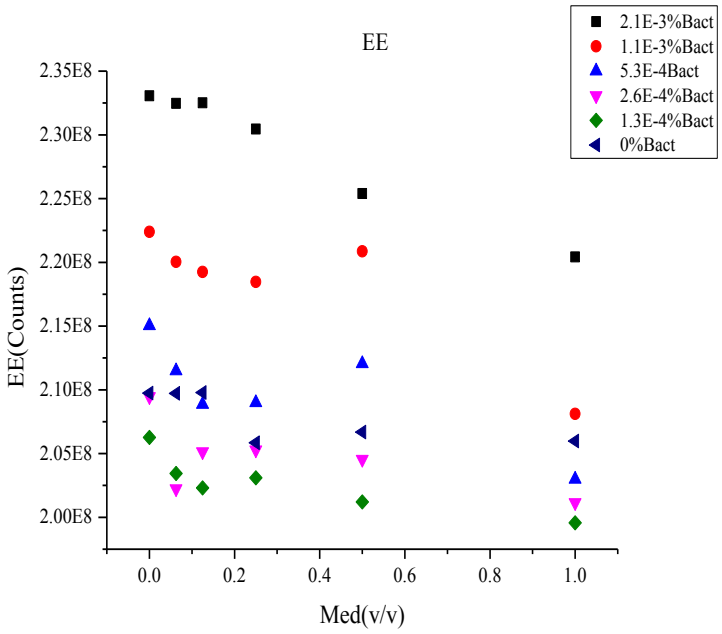

Fig. 7: A graph displaying the EE signal in photon counts versus the volume fraction of media for each of the series in the training set.

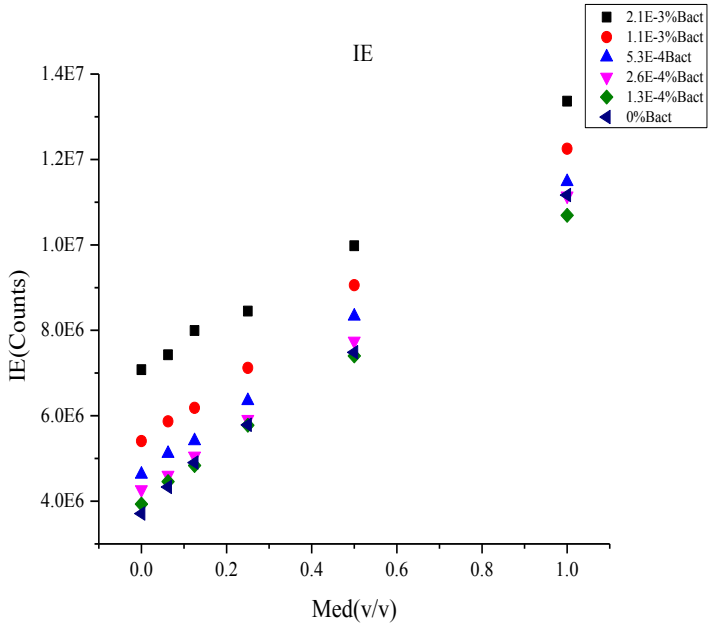

Fig. 8: A graph displaying the IE signal in photon counts versus the volume fraction of media for each of the series in the training set.

These data will be used to obtain the BSN parameters a-f in section 4 below.

Growth Curve

Given the parameters a-f, the BSN algorithm was applied to a realistic situation that occurs in laboratories and commercial bioreactors. Two *PA* growth curves were produced, one for six hours and the other for twelve hours. Before starting the twelve-hour experiment two UV-vis spectra were taken of the clean cuvette. The first with the cuvette orientated with the 'QS' facing the user, 90° from the light source the second with the initials away from the light source. The scans were performed in the full wavelength range capability of the Perkins-Elmer Lambda 950 spectrometer, 3300nm to 175nm, and were labeled blank 1 and blank 2 respectively. The same method used to calculate the EE and IE of the BSN spectra from the calibration curve and training set was used for the growth curves.

Analysis of Biofilm

Since we used OD_{600} as a bacterial number density measurement we decided to check on the possibility that the medium or the culture deposited a film on the walls of the cuvette that could frustrate the approach. Immediately after completing the twelve-hour growth curve and disposing of the bacterial culture each of the interior sides of the cuvette were washed drop-wise with 1mL of filtered PBS. Two UV-Vis scans were conducted with the cuvette empty. The first was labeled side 1 and the second side 2; side 1 corresponds with the same orientation of the cuvette as blank 1 and side 2 with blank 2. The spectra were measured using the same setting as with the blanks, the corresponding blanks were subtracted from the scans. And then the absorbance was plotted against the wavelength using the Origin program.

Figure 9 shows the UV-Vis spectra of the biofilm for both sides 1 (black) and 2 (red). The blue arrows correspond to probable fringes for side 1 and the inset shows the region where most of the fringes are located for both sides of the cuvette. For side 1 the fringes were located at about 400, 426, 453, 480, 508, 528, 536, 571, 536, 571, 625, 697, 796, 971, 1065 and 1195nm. And for side 2 they're located at about 348, 367, 382, 401, 427, 449, 476, 507, 553, 603, 649, 757, 857, 977 and 1148nm.

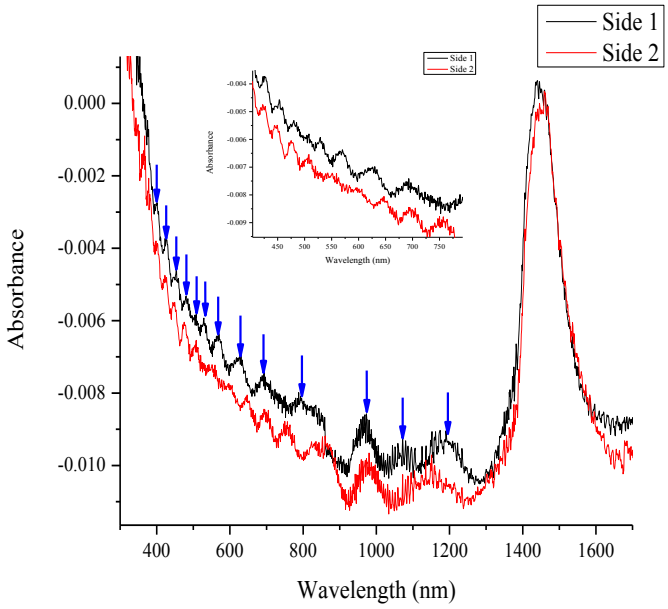

Fig. 9: UV-Vis spectra of biofilm for both sides 1 (black) and 2 (red). Blue arrows indicate fringes for side 1.

Based on the algorithm of Goodisman and Chaiken[16] the optical thickness of the thin films responsible for the interference fringes are 3839 nm and 3535 nm for sides 1 and 2 respectively. This represents an 8% variation but it is known that the films were not measured simultaneously and also that the apparent thickness is a strong function of water content. The absorption feature

at 1451 cm^{-1} is slightly larger for side 1 than side 2 indication slightly more water in side q than side 2 consistent with the 8% variation containing some systematic variation due to drying. The presence of these films suggests that attempts to do absorption measurements on a fluid phase in a cuvette will also have a contribution from films to the observed spectra.

Baseline Correction for Raman Spectra

A baseline correction called a "101-7" was performed on the Raman spectra so that peaks can be more easily observed for comparison. This was done by first summing up the signals of every 20-minute series of scans for each of the wavenumbers from 901cm^{-1} to 1901cm^{-1} and transferring that data with their corresponding wavenumbers to an Origin worksheet. The 101-7 baseline subtraction involves first smoothing the experimental spectrum using simple 101 point adjacent averaging. The smoothed spectrum resembles the underlying fluorescence spectrum and is then subtracted from the experimental spectrum to leave the more narrow Raman features. The difference i.e. the Raman spectrum is then smoothed using a 7 point adjacent averaging window to reduce high frequency noise thereby producing a "101-7 baseline corrected spectrum". Figure 11 shows the baseline corrected Raman spectra displaying all possible chemical peaks more clearly than the raw spectra shown in Figure 10. Operational details on the 101-7 baseline correction can be found in the Appendix.

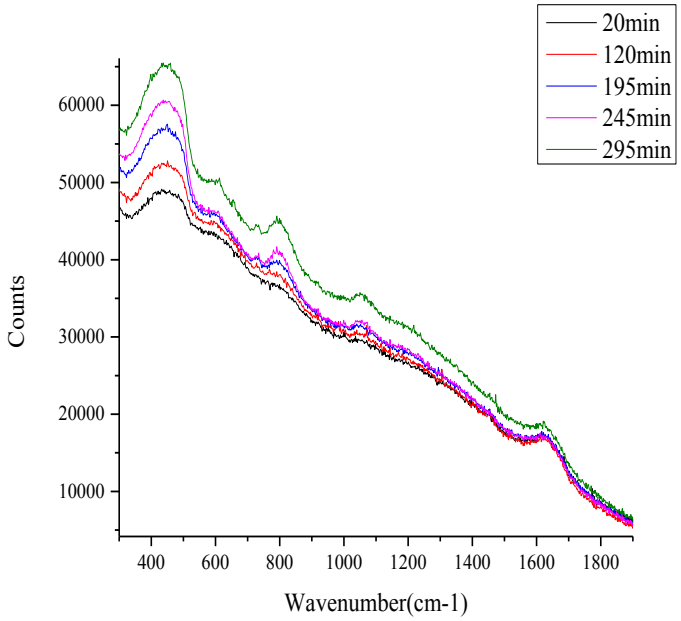

Fig. 10: The Raman spectra for the six-hour growth curve.

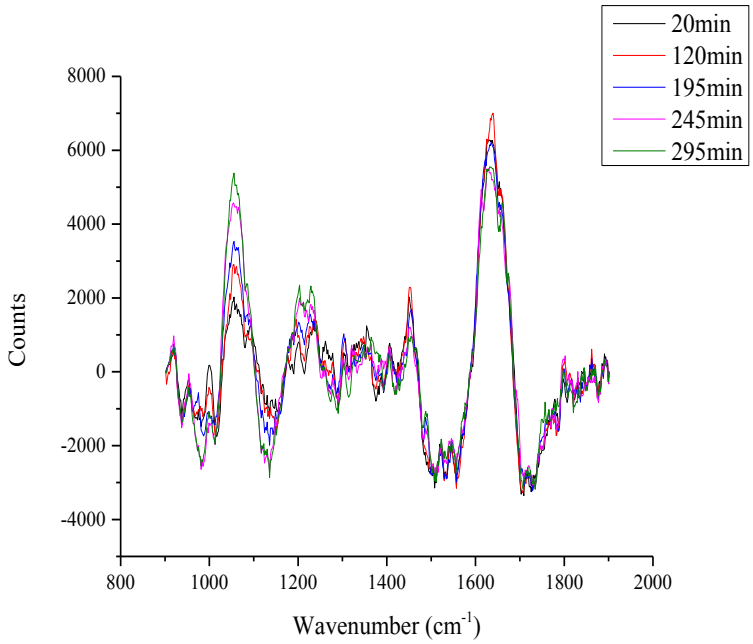

Fig. 11: The Raman spectra after the 101-7 baseline correction for the six-hour growth curve showing possible chemical peaks.

All baseline subtraction procedures make assumptions about the fluorescence and Raman region of the spectra.[17] In our case one such assumption is that Raman features (including clusters of congested Raman peaks) are narrow, most often narrower than 200cm^{-1} wide. The 101-point smoothing used in this procedure corresponds to approximately a 200cm^{-1} range. This produces a baseline that roughly bisects only the Raman contribution to the spectra above the contribution from the sum of the fluorescence and unresolved Raman due to spectral congestion. As a result peaks that are narrower than 200cm^{-1} are reproduced in the corrected spectra without distortion and the 101-point smoothed spectra that is subtracted from the raw data will decrease the contribution from unresolved Raman and fluorescence features. The artifacts produced by this and all other baseline subtraction procedures are discussed in the literature.[18] In general, the dividing line between fluorescence emission and Raman emission is not usually known with any precision.

As a preliminary to Chemometric Analysis we performed some crude integration of peaks that were obviously varying in a systematic manner. The 1066cm^{-1} peak was integrated using the baseline corrected spectra at five time intervals (20, 120, 195, 245 and 295min). Then the graph was cropped to show only the region from 950cm^{-1} to 1150cm^{-1} and a line was drawn from 1014cm^{-1} to 1075cm^{-1} (Figure 12 black line) this range was chosen so as to include as much of the peak without including the possible peak at 1120cm^{-1}. The counts corresponding to the horizontal line were subtracted from the signals along that line and the results were summed up to find the area of the peak. This procedure was repeated for the peak at 1120cm^{-1} for the region from 1097cm^{-1} to 1148cm^{-1} (Figure 12 red line). While Figure 13 is the spectra of D-Glucose at

varying concentrations and Figure 14 are the spectra of DL-dipalmitoylphosphatidylcholine representing biomass. Figure 15 and 16 display the change in areas for both the 1066cm^{-1} and 1120cm^{-1} peaks as a function of time. This procedure has been shown[16] to give good correlation with calibration curves for solutions containing known amounts of analytes e.g. glucose in PBS as in Figure 13.

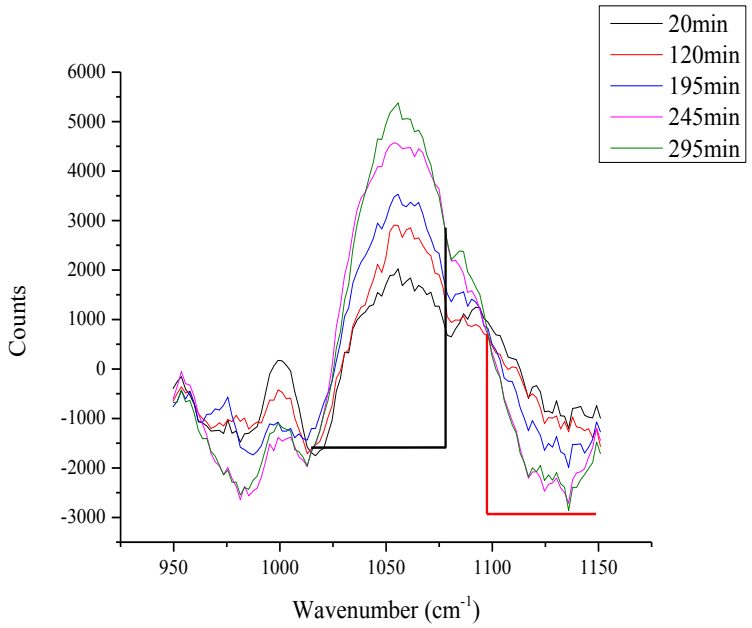

Fig. 12: The baseline corrected spectra showing the range of the peak integration at 1066cm^{-1} (black) and 1120cm^{-1} (red).

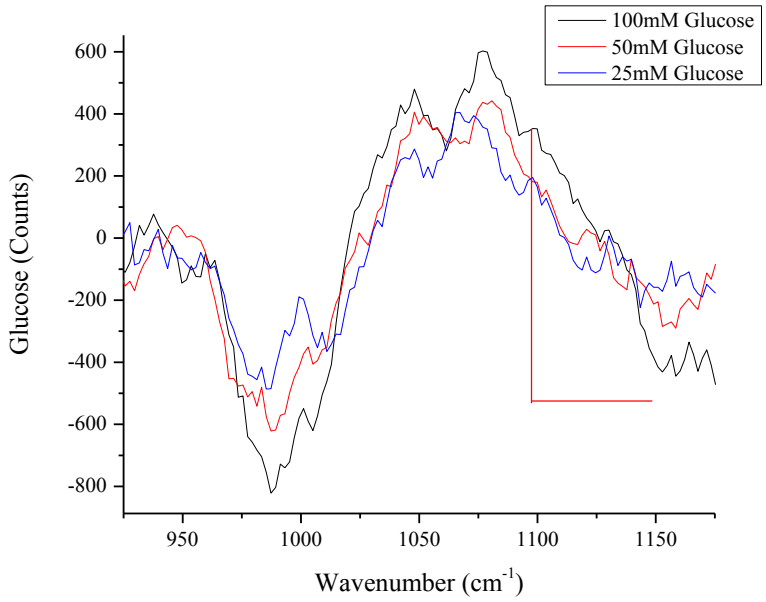

Fig. 13: The spectrum of glucose in water showing the peak at about 1120cm^{-1}.

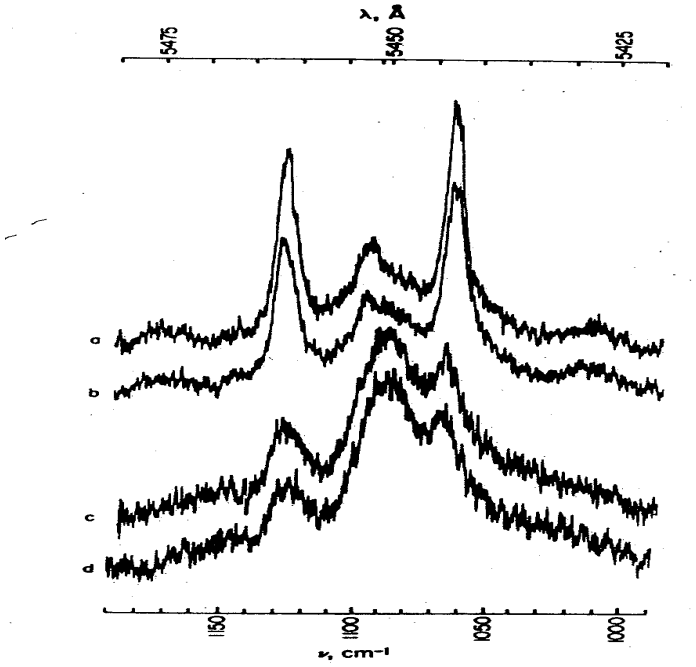

Fig. 14: The Raman spectrum of 20% DL-dipalmitoylphosphatidylcholinesonicates in water showing the peak at about 1066cm^{-1}. This scan was taken at various temperatures (a) 20°C (b) 30°C (c) 40°C (d) 50°C.[19]

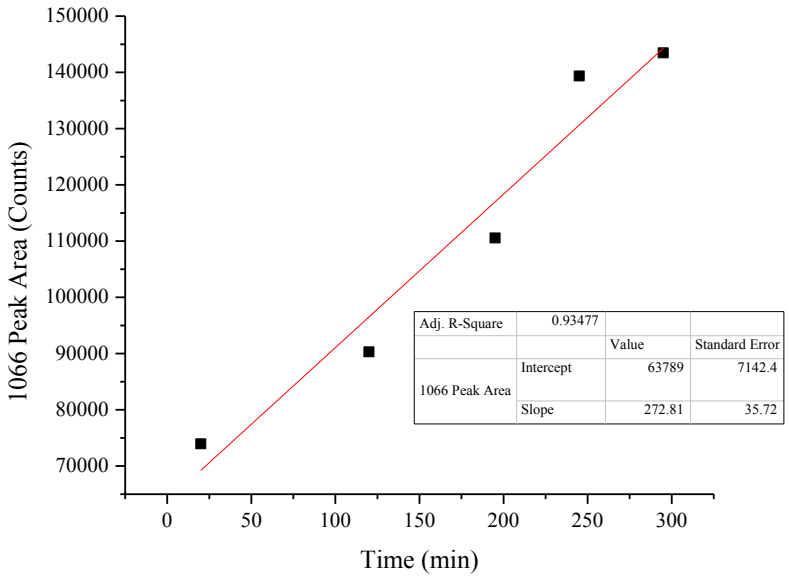

Fig. 15: A graph of the peak sizes at 1066cm^{-1} versus time for the six-hour growth curve.

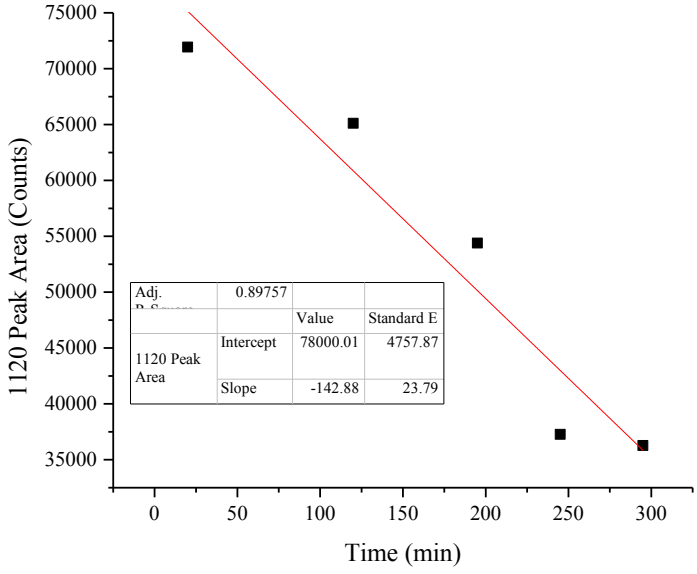

Fig. 16: A graph of the peak sizes at 1120cm^{-1} versus time for the six-hour growth curve.

Results

Bilinear Regression Fit

A bilinear regression fit was applied to the training set by first converting the OD_{600} for each of the solutions to volume fraction of bacteria this was called the OD_{600} volume fraction of bacteria (OD_{600} Bact) using equation [7]. Origin was used to plot the actual volume fraction of bacteria as the dependent variable and both the corresponding EE and IE as independent variables in accordance with equation [5]. From the fitting option in the analysis menu of the Origin program, multiple regressions fit was selected and the program returned a bilinear fit and r^2 value. This process was repeated for the actual volume fraction of media diluted with PBS and the same EE and IE signals used for the bacteria bilinear fit. Below are the equations for both the volume fraction of bacteria and the volume fraction of media bilinear fit.

$$\phi_{bac} = -1.23569\times10^{-4} + 6.03667\times10^{-13}EE + 7.1214\times10^{-13}IE \qquad [8]$$

$$\phi_{med} = -6.48981 + 3.0785\times10^{-8}EE + 4.01596\times10^{-8}IE \qquad [9]$$

Equations [8] and [9] are used to calculate the volume fractions of bacteria ϕ_{bac} and media ϕ_{med} employing only the measured EE and IE quantities. These values were called the "BSN Bact" and "BSN Med". The BSN Bact was plotted against the actual values from the OD_{600} to produce the graphs in Figure 17. However the OD_{600} does not give information on the media concentration so the BSN Med is compared to the dilution factor used in the training set to produce Figure 18.

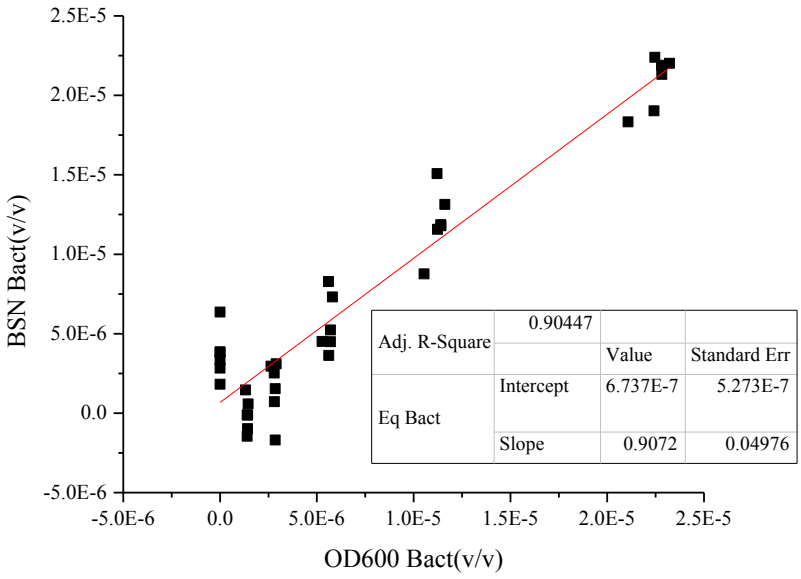

Fig. 17: A plot of the BSN volume fraction of bacteria versus the OD_{600} volume fraction of bacteria. The data corresponding to 0.0 v/v has a higher BSN bacteria concentration than the two following series because of the light scattering from the bottom of the cuvette.

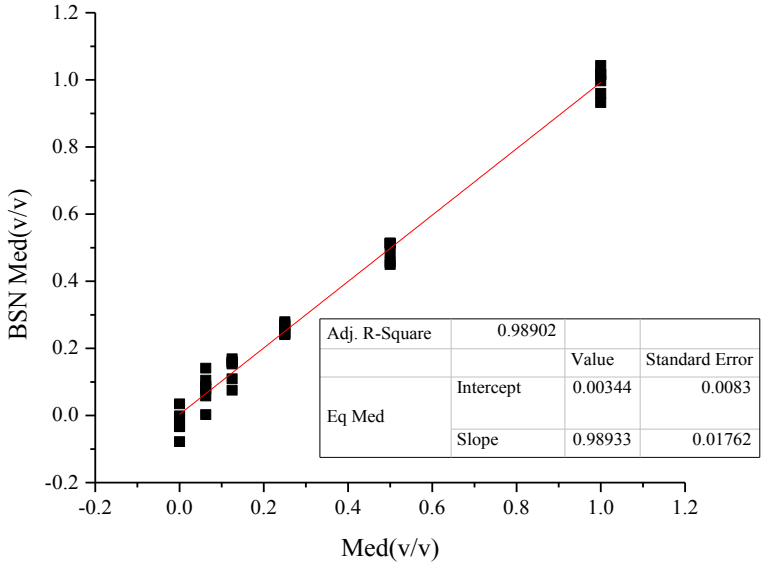

Fig. 18: A plot of the BSN volume fraction of media versus the media composition by dilution factor.

PA Growth Analysis

Next we applied the calibrated BSN algorithm obtained from the training set to the *PA* growth to find ϕ_{bac} and ϕ_{med} respectively from the EE and IE signals obtained from the growth curves. Then the results were plotted versus time and a growth curve was created using the UV-Vis data so that they can be compared. Figures 19-22 display the growth/decay curves and the comparison of calculated versus actual volume fractions for six hours and Figures 23-26 for twelve hours.

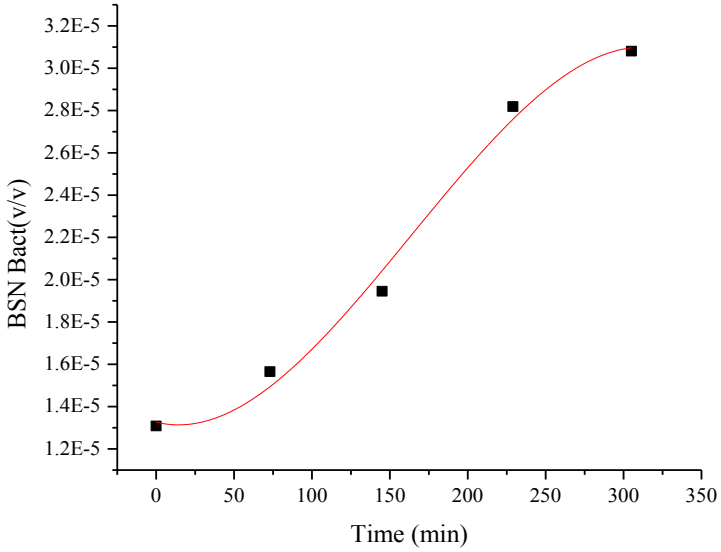

Fig. 19: Volume fraction of bacteria from the BSN algorithm versus time for six-hour growth curve. The red line serves as a guide only.

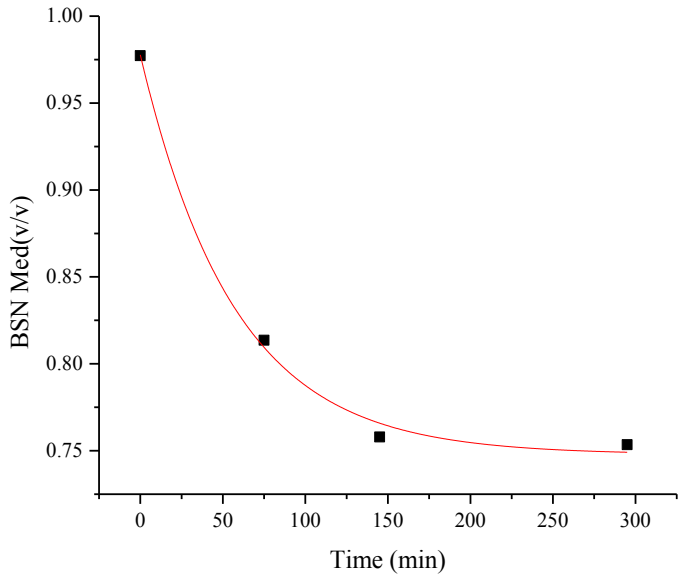

Fig. 20: Volume fraction of media from the BSN algorithm versus time for six-hour growth curve. The red line serves as a guide only.

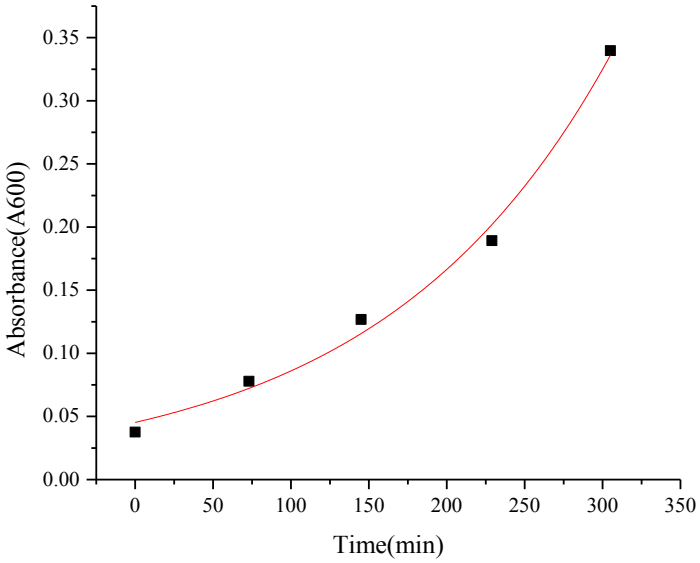

Fig. 21: Absorbance at 600nm versus time for the six-hour growth curve. The red line serves as a guide only.

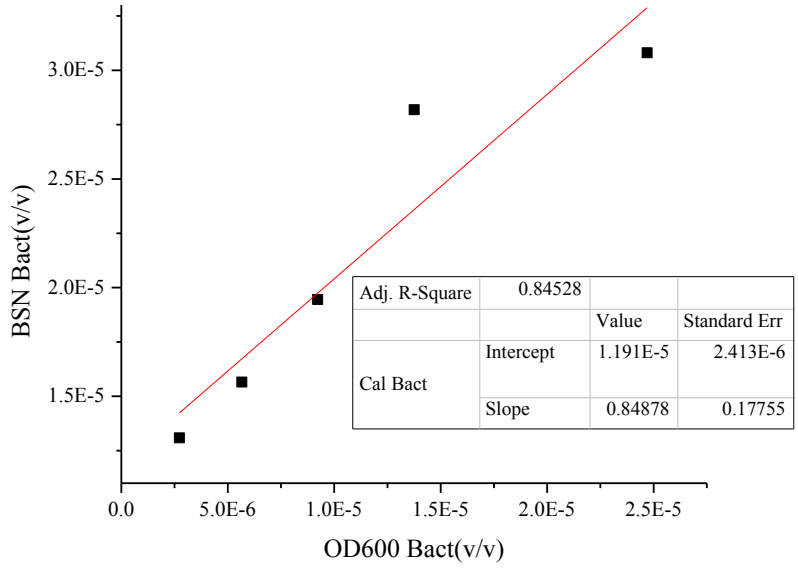

Fig. 22: A graph displaying the BSN ϕ_{bac} versus OD_{600} ϕ_{bac} for the six-hour growth curve.

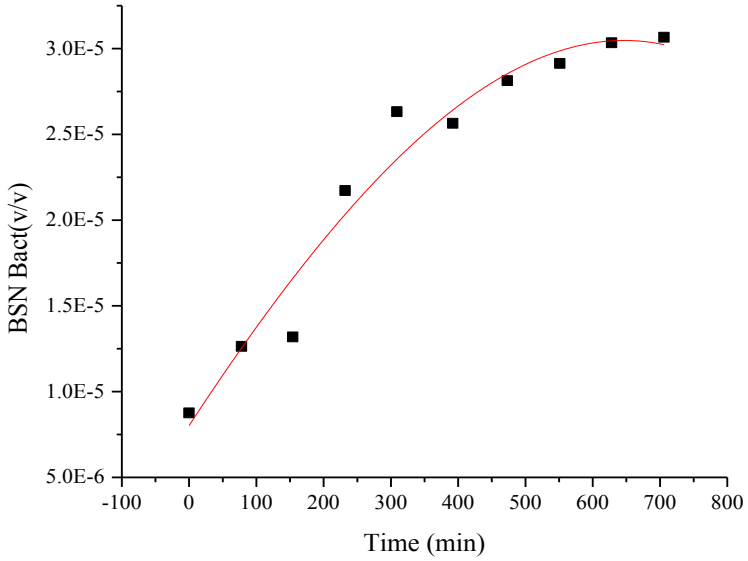

Fig. 23: Volume fraction of Bacteria from the BSN algorithm versus time for twelve-hour growth curve. The red line serves as a guide only.

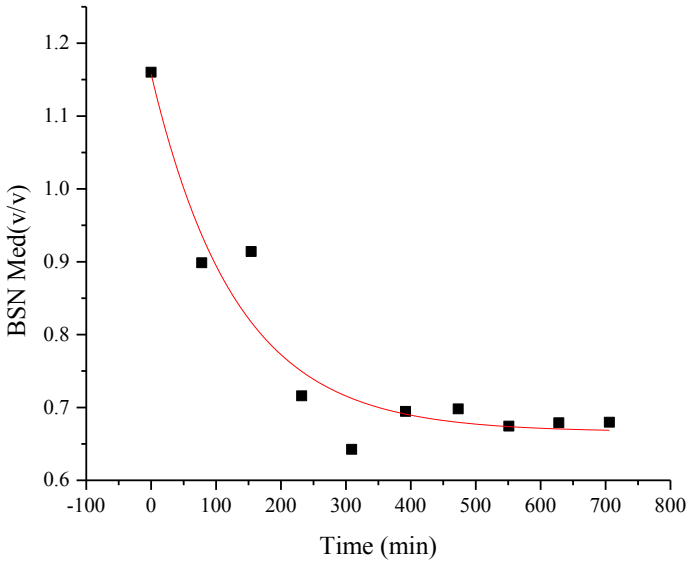

Fig. 24: Volume fraction of Media from the BSN algorithm versus time for twelve-hour growth curve. The red line serves as a guide only.

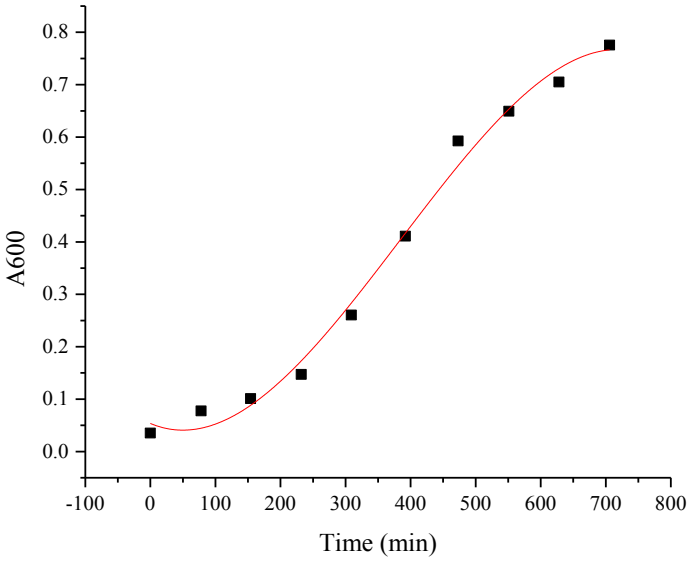

Fig. 25: Absorbance at 600nm versus time for twelve-hour growth curve. The red line serves as a guide only.

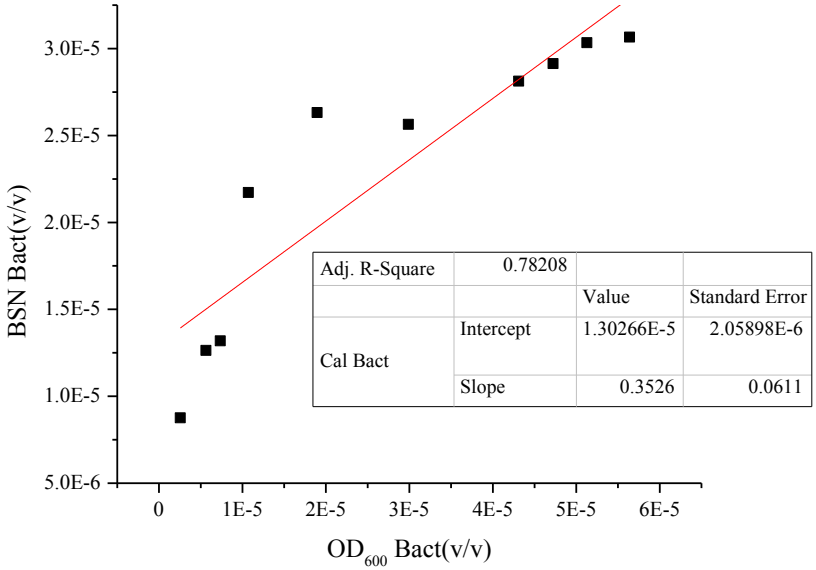

Fig. 26: A graph displaying the BSN ϕ_{bac} versus OD_{600} ϕ_{bac} for the twelve-hour curve.

Discussion

Figures 17 and 18 demonstrate the validity of the BSN algorithm, with the OD_{600} ϕ_{bac} and ϕ_{med} plotted against their respective calculated values from equations [8] and [9] the slope would be expected to be 1 and the intercept at 0. This is what we see in Figures 17 and 18 with slopes of 0.9045 ± 0.04976 and 0.989 ± 0.01762 respectively and the intercepts were $6.74 \times 10^{-7} \pm 5.27 \times 10^{-7}$ and 0.0034 ± 0.0083 counts respectively. However for the bacteria (Figure 17) excluding the 0.0v/v series since this is the light scattering by the cuvette the r^2 value would be 0.949, a slope of 0.996 ± 0.0428 and an intercept of $-6.98 \times 10^{-7} \pm 4.96 \times 10^{-7}$ counts. This is attributed to the accuracy of the algorithm. Another aspect of the graphs that show the validity of the BSN algorithm is the grouping of the data points. The precision of the algorithm is displayed by the close grouping of the data points that distinctly show each of the series of the training set.

When applied to the six-hour growth curve the trend in the bacteria concentration obtained from the BSN (Figure 19) closely resembles the growth curve produced from the OD_{600} (Figure 21). Just like with the training set the BSN and OD_{600} ϕ_{bac} were plotted against each other to produce Figure 22. From Figure 22 we can see that despite the presence of an outlier that there is a linear correlation between BSN and OD_{600} ϕ_{bac} excluding the outlier the r^2 value is 0.993.

As for the 12 hour growth (Figure 23) shows the increase in the bacteria concentration derived from the BSN as the growth progresses much like the OD_{600} (Figure 25). And the volume fraction of media for both the 6 hour (Figure 20) and 12 hour (Figure 24) growth curves are decreasing exponentially. Figure 26 that displays the BSN versus OD_{600} ϕ_{bac} for the 12 hour growth curve shows that the trend is very close to being linear and that the linearity in the trend stops about halfway. This corresponds to an OD_{600} of about 0.4 according to Figure 25, when creating the calibration curve an OD_{600} of about 0.4 was determined to be the end of the linear range of concentration as related to the EE and IE signals. Only including the first five data points of Figure 26 gives a linear graph with r^2 value of 0.904.

In addition to allowing users to find bacteria concentration in liquid media the Raman spectra from the same scans permits the extrapolation of the chemical change in the solution. Figure11 shows the potential peaks from chemical species in the solution. Many of these peaks will have to be identified experimentally but there are some peaks that we hypothesize correspond to certain substances. One such peak is the broad one at about 1066cm^{-1} that might be caused by the lipids in the cell membranes, as well as the region about 1120cm^{-1} that we believe to correspond

to glucose.[16] Figure 12 shows this region of the spectra in greater detail along with the ranges for the integration of the peaks at both 1066cm^{-1} and 1120cm^{-1}.

The change in areas for these peaks are shown in Figures 15 and 16, a negative correlation between the two peaks can be clearly seen based on the literature spectra/results these peaks corresponded to the cells' lipid bilayer membranes (1066cm^{-1})[19] and glucose (1120cm^{-1})[16]. If true, the assignment to lipid bilayer is convenient since it gives a sense of the amount of biomass being produced independent of the concentration of individual organisms i.e. if the average size of the bacteria change while their number density doesn't, then we can expect an increase in biomass as indicated by the strength of the 1066cm^{-1} feature while the bacteria concentration does not change in concert.

Another peak of interest is the one at 1600cm^{-1} that corresponds to water; as the cell concentration increases they displace the water molecules. This is shown in the spectra (Figure 11), the largest 1600cm^{-1} peak is the one at 120min and then it decreases as time progresses. Examining the BSN volume fraction of media for the 6 hour (Figure 20) and 12 hour growth curves (Figure 24) shows this as well; the longer the cells are allowed to grow the lower the volume fraction of media.

Finally we observe the systematic increase in a Raman feature close to 800cm^{-1}. This could be associated with the anomeric carbon in glucose and similar hexose polymers. Since the *PA* produces conspicuously slimy fluid growth media we speculate that the growing Raman feature could be associated with that material. Much more work remains to be done but clear systematic

variation of at least 4 distinct Raman features offers the possibility of revealing new insights into *PA* bacterial cultures and their local chemical environs.

The UV-Vis spectra of the *PA* biofilm (Figure 9) showed that a small but insidious error could be introduced into bacterial measurements based on OD_{600} *in situ* due to independently variable losses that would mask absorptions due to biofilm formation. On the other hand analysis[16] of the fringes gives the optical thickness, an important parameter in current biofilm research. The fringes arise from the interference between photons that are repeatedly reflected within the walls of the biofilm. The thickness of the biofilm determines whether the reflected photon will interfere with the incident light constructively or destructively at certain wavelengths. An even number of half wavelengths per round trip within the film would interfere constructively and an odd number would be destructive. This information together with the refractivity of the biofilm is now available using an algorithm developed by Chaiken and Goodisman using spectroscopy alone and without having to use CV dye.[16]

Along with the identification of the spectra peaks future works will have to include the affect on the spectra by a change in the presence of different chemicals, such as adding deuterated water. A study into the affect on ϕ_{bac} and ϕ_{med} as the bacteria cells produce biofilms will also have to be conducted. This method will have to be compared to other bacteria such as *E.coli* and *S.oneidensis*. For each of these bacteria a training set and bilinear fit equation will have to be developed. When *PA* is exposed to environmental stress it tends to escalate the production of the biofilm in order to survive.[10] The Raman spectra and the BSN can provide information on the initial and intermediate chemical changes for the production of these biofilms.

Conclusion

The data from this study confirms the ability to simultaneously both cell population and quantitative chemical information noninvasively from bacterial cultures in the real time without the use of chemical labels. The BSN algorithm was shown to simultaneously monitor the cell concentration and provide Raman spectra of metabolic feedstock i.e. glucose and anabolic products e.g. phospholipid membranes. This is qualitatively improved information in that users can collect data from one instrument with little sample preparation and perfect temporal and spatial registration of the two types of measurements in a bacterial population. These results suggest that researchers may be able to develop new applications involving the BSN method in bioreactor design and process optimization. Alternatively the real time i.e. 20msec time scale response of cells to potential biofilm inhibiting agents or simply a population's chemical consumption and production in response to different environmental stressors e.g. low or high temperature or low nitrogen availability are also viable potential applications of this simple but versatile algorithm.

Appendix

To produce the 101-7 baseline corrected spectra first sum up the signals of every 20-minute series of scans for each of the wavenumbers from 901cm^{-1} to 1901cm^{-1} and transferring that data with their corresponding wavenumbers to an Origin worksheet. Then three new columns were created in the worksheet. Highlight the first column of the signal data by clicking the top of the column, from the analysis menu go to the signal processing option then smooth and select open dialog. In the signal-processing window select adjacent averaging from the method drop down

menu. Type in 101 in the points of window field and select the first newly created column as the output by clicking on the adjacent arrow and selecting the column. This will automatically place the results of the 101-point averaging in the first new column. Highlight the second new column and press control Q on the computer keyboard; this brings up the set values window. Then subtract the 101-point averaging from the original data, example Col(B)-Col(Y). With the second new column highlighted perform another smoothing with a 7-point averaging by entering 7 in the points of window field and selecting the third new column as the output. This will be the final result of the 101-7 corrections and was repeated for each set of data then were plotted against the wavenumbers to create Figure 11

References

[1] J. Chaiken, et al, "Analyzing near-infrared scattering from human skin to monitor changes in hematocrit", *Journal of Biomedical Optics*, 16(9), 1-19 (2011).

[2] V. Tuchin, *Tissue Optics: Light Scattering Methods and Instruments for Medical Diagnosis*, SPIE Press, Bellingham, WA, 2000.

[3] J.W. Costerton, P.S. Stewart and E.P. Greenberg, "Bacterial Biofilms: A Common Cause of Persistent Infections", *Science*, 284(5418), 1318-1322 (1999).

[4] J.B. Lyczak, C.L. Cannon and G.B. Pier, "Establishment of *Pseudomonas aeruginosa* Infection: Lessons From a Versatile Opportunist", *Microbes and Infection*, 2, 1051-1060 (2000).

[5] X. Wu, et al, "Culture-free diagnostics of *Pseudomonas aeruginosa* infection by silver nanorod array based SERS from clinical sputum samples", *Nanomedicine: NBM*, 1-8 (2014).

[6] H. Chai, et al, "Spectroscopic investigations of the binding mechanisms between antimicrobial peptides and membrane models of *Pseudomonas aeruginosa* and *Klebsiella pneumonia*", *Bioorganic & Medicinal Chemistry*, 4210–4222 (2014).

[7] E.E. Mann and D.J. Wozniak, "*Pseudomonas* biofilm matrix composition and niche biology", *FEMS Microbiol. Rev.* 36, 893-916 (2012).

[8] S. E. F. Borgos, et al, "Rapid metabolic profiling of developing *Pseudomonas aeruginosa* biofilms by high-resolution mass spectrometry fingerprinting", *Ann. Microbiol.* 1-8 (2014).

[9] Q. Wei and L. Z. Ma, "Biofilm Matrix and Its Regulation in *Pseudomonas aeruginosa*", *Int. J. Mol. Sci.*14, 20983-21005 (2013).

[10] H.M. Al-Qadiri, et al, "Rapid Detection and Identification of *Pseudomonas aeruginosa* and *Escherichia coli* as Pure and Mixed Cultures in Bottled Drinking Water Using Fourier Transform Infrared Spectroscopy and Multivariate Analysis", *J. Agricultural and Food Chemistry* 54, 5749-5754 (2006).

[11] M. Arabski, S. Wąsik, and Z. Drulis-Kawa, "Laser Interferometry Analysis of Ciprofloxacin Diffusion through *Pseudomonas aeruginosa* Biofilm", *Clin. Microbiol*. 2, 105-110 (2013).

[12] D.K. Shen, et al, "PsrA is a Positive Transcriptional Regulator of the Type III Secretion System in *Pseudomonas aeruginosa*", *Infection and Immunity* 74(2), 1121-1129 (2006).

[13] D.K. Shen, et al, "High-Cell-Density Regulation of the Pseudomonas aeruginosa Type III Secretion System: Implications for Tryptophan Catabolites", Microbiology 154, 2195-2208 (2008).

[14] M. Baniasadi, et al, "Nano indentation of *Pseudomonas aeruginosa* bacterial biofilm using atomic force microscopy", *Materials Research Express 1*, 1-15 (2014).

[15] O. Stukalov, et al, "Use of Atomic Force Microscopy and Transmission Electron Microscopy for Correlative Studies of Bacterial Capsules", *Appl. Environ. Microbiol.* 74(17), 5457-5465 (2008).

[16] R. T. McDonough, et al, "Label-free characterization of optical thickness and hydration of native microbial biofilms using interference fringes and near IR absorption", Manuscript in preparation.

[17] C. A. Lieber and A. Mahadevan-Jansen, "Automated Method for Subtraction of Fluorescence from Biological Raman Spectra", *Appl. Spectrosc.* 57, 1363-1367 (2003).

[18] T. Saxena, et al, "Raman spectroscopic investigation of spinal cord injury in a rat model", *Journal of Biomedical Optics*, 16(2), 1-14 (2011).

[19] A. T. Tu, *Raman Spectroscopy in Biology: Principles and Applications*, "Lipids and Biological Membranes", John Wiley & Sons, New York, NY, 1982.

Vita

Steven Ortiz

Chaiken Research Group, Department of Chemistry, Syracuse University, 0-012 Center for Science and Technology, Syracuse, NY 13210

Work Experience

Teaching Assistant in Chemistry	Syracuse University	September 2013 – Present
Chemistry Lab Technician	Interplex Engineered Products	November 2012 – July 2013
Physical Sciences Tutor	Rhode Island College	September 2010 – May 2012

Research Experience

Graduate Research Assistant	Syracuse University	December 2013 - Present
Undergraduate Research Assistant	Rhode Island College	May 2011 - December 2011

Teaching Experience

As Teaching Assistant at Syracuse University

General Chemistry I Laboratory

General Chemistry II Laboratory

Publication/Presentation

S. Ortiz and K. H. Almeida, “Molecular Dimerization State of NAMPT”, Poster presentation at the Rhode Island Summer Research Program for Undergraduates (RI-INBRE).

Education

Master of Science in Chemistry	Syracuse University	September 2013 – December 2015
Bachelor of Science in Chemistry	Rhode Island College	January 2010 – May 2012